Data fusion for reconstruction of a DTM, under a woodland canopy, from airborne L-band InSAR

Clare S. Rowland and Heiko Balzter

Abstract— This paper investigates the utility of different parameters from polarimetric interferometric SAR data for the identification of ground pixels in a woodland area to enable accurate digital terrain model (DTM) generation from the InSAR height of the selected ground hit pixels. The parameters assessed include radar backscatter, interferometric coherence, surface scattering proportion (based on Freeman-Durden decomposition) and standard deviation of the interferometric height. The method is applied to Monks Wood, a small semi-natural deciduous woodland in Cambridgeshire, UK, using airborne E-SAR data collected in June 2000. The 1428 variations of SAR-derived terrain models are validated with theodolite data and a LiDAR-derived DTM. The results show that increasing the amount of data used in the DTM creation does not necessarily increase the accuracy of the final DTM. The most accurate method, for the whole wood, was a fixed window minimum filtering algorithm, followed by a mean filter. However, for a spatial subset of the area using the υ_3 backscattering coefficient to identify ground pixels out-performs the minimum filtering method. The findings suggest that backscatter information may often be undervalued in estimating terrain height under forest canopies.

***Index Terms*— polarimetric interferometric synthetic aperture radar (PolInSAR), vegetation, digital terrain model (DTM), ancillary data, interferometry, polarimetry**

I. Introduction

InSAR is an established technique that allows the estimation of elevation from the phase difference between two overlapping images acquired from slightly different sensor positions [1]. InSAR sensors record the phase and the amplitude of the backscatter return, with the difference in phase between the two images being related to the difference in path length to a point and therefore its location. Polarimetric data is sensitive to the orientation of the elements within a pixel and may be recorded at co-polarized HH (horizontal transmit, horizontal receive), VV (vertical transmit, vertical receive) and cross-polarized HV or VH polarizations (transmitted in one orientation, received in the other). Fully polarimetric data sets, where HH, HV, VV and VH polarizations are recorded, enable more information about the scattering processes to be determined, particularly through polarimetric decomposition [2]-[4].

Incorporating polarimetric data into SAR interferometry enables information on the scattering processes and their height to be determined. Applications of polarimetric SAR interferometry (PolInSAR) have focused on forested areas, but have also explored the potential for PolInSAR analysis over agricultural and urban areas [5], [6] and snow [7]. Forest height mapping is the most developed PolInSAR application area with work focusing primarily on model development and model inversion to yield canopy height, topography and canopy extinction rates [8]-[10]. The more independent observations used to invert these simplified models, the better the resulting estimate of canopy height becomes, with multiple polarizations, multiple baselines or multiple wavelengths all valuable additional sources of information [11], [12].

Estimates of canopy height from radar and airborne laser scanner data can be derived in a number of ways. One method is to use a digital surface model (DSM) to map the height of the top of the canopy and a digital terrain model (DTM) to give the height of the underlying terrain. The difference between the DSM and DTM provides the estimate of canopy height. This approach has been successfully applied to dual wavelength InSAR data [13], [14] and LiDAR discrete-return data for a deciduous woodland [15]. The accuracy of the height estimates is dependent upon the accuracy of the DSM map of canopy height, which depends mainly upon the degree of signal penetration, and the accuracy of the DTM, which maybe poor, especially under dense canopies.

In cases where a suitable DTM can not be derived from available remote sensing data existing topographic maps have proved useful, in conjunction with InSAR derived large-scale DSM's [16], [17]. Large-scale InSAR DSM's are now available, with the Shuttle Radar Topography Mission (SRTM) product, which was flown in February 2000, mapping 80% of the Earth's land surface with a C-band (5.6cm) InSAR to produce an almost global DSM at ~30m (1 arc second) resolution in the US and ~90m (3 arc seconds)

Manuscript received October 18, 2006. This study was supported by the UK Natural Environment Research Council (NERC) under the New Observing Techniques Programme, CORSAR project, Grant number NER/Z/S/2000/01282.

C. S. Rowland is with the Centre for Ecology & Hydrology Monks Wood, Huntingdon, Cambridgeshire, PE28 2LS, UK. (email: clro@ ceh.ac.uk).

H. Balzter was with the Centre for Ecology & Hydrology Monks Wood, Huntingdon, Cambridgeshire, PE28 2LS, UK. He is now with the Department of Geography, University of Leicester, Bennett Building, University Road, Leicester, LE1 7RH, UK (email: hb91@leicester.ac.uk).

resolution elsewhere [18]. Airborne InSAR systems are also being used to generate large-scale DSM products, notably NEXTMAP produced by Intermap with their X-band (~3cm) Star-3i system [19].

The generation of DTM's from DSM's is problematic in regions with forest or urban land cover, as the influence of tree canopy and buildings needs to be removed or minimized to avoid contaminating the DTM. A number of methods have been investigated to derive DTM's from InSAR DSM's, with [20] investigating rules for the automatic generation of DTM in urban areas. Whilst ground height estimates are produced by inversion of some InSAR canopy models they have not generally been exposed to the rigorous validation applied to the canopy height products [8]-[11]. Creation of DTM's under forest canopies has been mainly the preserve of the airborne laser scanning community (for example [21]-[24]). Data fusion methods are beginning to be explored for the improvement of InSAR and LiDAR DTM's, such as using the interferometric coherence to identify areas where an InSAR DTM performs poorly and filling those gaps with elevation from a stereoscopic SAR DTM [25]. Multi-spectral and LiDAR have been successfully combined to produce a sophisticated method of building detection to enable more accurate generation of urban DTM's from LiDAR data sets [26].

PolInSAR data sets comprise a number of parameters, including polarization, wavelength, interferometric phase, interferometric coherence, backscatter intensity and spatial (or textural) information. In many applications only a single parameter out of this family is exploited. This paper proposes a method for incorporating ancillary data sets into the generation of InSAR DTM's for areas under forest canopies and assesses the utility of various data sets for identifying ground pixels. We define a ground pixel as a pixel where the primary influence on the interferometric phase is the ground and hence where the pixel can be identified by the dominance of surface scattering in the InSAR signal. The method is tested at a temperate, semi-natural deciduous wood.

This paper is organized as follows: Section II describes the study site and data sets, and is followed by Section III which outlines the DTM production method, while Section IV covers the validation method. Section V presents the results and is followed by the discussion and conclusions in Sections VI and VII respectively. In this paper we use the following definitions: The DTM is the elevation of the terrain, including terrain underlying vegetation or urban areas. The DSM is the 'raw' elevation product from the sensor in question and includes the height of vegetation albeit with some underestimation due to signal penetration into the canopy.

II. STUDY SITE AND DATA SETS

A. Study site

Monks Wood (52°24'N, 0°14'E) is a semi-natural deciduous woodland located in south-east England, UK and covers 157ha. The principal overstorey species are ash, maple and oak, with main understorey species including hawthorn, hazel and blackthorn. The maximum tree height is around 26m and the mean tree height is about 12m. Terrain elevation varies from 6m to 46m, with a maximum slope angle of 14.5° [27]. Canopy cover varies from completely open along rides and two fields, within the woodland perimeter, to completely closed. The wood is divided into stands, by rides and paths through the wood, but the stands are heterogeneous in terms of overstorey and understorey density, tree age distribution and species composition.

B. InSAR data and processing

A fully polarimetric L-band InSAR data set of Monks Wood was acquired by the airborne E-SAR sensor on 1st June 2000. The L-band (23cm wavelength; 1.3 GHz) data were repeat-pass with a temporal baseline of 13 minutes and a horizontal and vertical baseline of approximately 10m and 0.4m respectively. The flight altitude was roughly 3km producing a ground range pixel size of 1.49m in the range direction and 0.85m in the azimuth direction. The data were multi-looked during the interferometric processing by 2 and 4 looks in the range and azimuth directions correspondingly. The InSAR processing produced a data set with a vertical accuracy of around 2m (e.g. L-HH root mean square elevation error of 1.95m against 14 bare ground control points). The incidence angle range across the wood is 39º – 54º. All InSAR raster data products were geocorrected to enable comparison with georeferenced theodolite and LiDAR data sets.

The fully polarimetric nature of the SAR interferometry data set enabled the three optimized coherence channels to be derived in addition to the L-HH, L-HV and L-VV polarizations based on the method developed by [8]. The method involves determining the optimum scattering mechanisms in polarimetric SAR interferometry data by maximizing the interferometric coherence. Twinned with a coherent decomposition algorithm it allows separation of the scattering phase centre heights for the optimum scattering mechanisms, resulting in three pairs of scattering mechanisms [8].

In the optimized coherence polarization basis the first singular value (υ_1) has the highest coherence and therefore typically contains the highest proportion of surface scatter. The third singular value (υ_3) has the lowest coherence and as such generally represents volume scattering, or a combination of volume scattering and surface scattering [28]. The coherence for the second singular value (υ_2) is an intermediate stage and is likely to feature a higher level of canopy scattering than υ_1 [28].

C. Theodolite data

A set of reference theodolite data, containing terrain elevation measurements at 244 points, were collected in June 2000 using a Pentax R-125N electronic total station (laser theodolite). The x, y and z co-ordinates of each point were

calculated in relation to a permanent Ordnance Survey benchmark located at the Centre for Ecology and Hydrology (CEH) Monks Wood research station. The terrain elevation points comprised of 140 measurements under the canopy, with the remaining 104 in open areas of the wood [15].

D. LiDAR-derived DTM and canopy height model

On 10th June 2000 the small-footprint airborne laser terrain mapper (Optech ALTM 1210) was flown over Monks Wood. The ALTM operates at 1047nm (near-infrared) and on average recorded one point (with a diameter of 0.25m) per 4.83m^2, with a minimum point density of 6.50m^2 and a maximum of 2.80m^2 in areas of swath overlap [15]. The first and last returns were recorded enabling a DTM and canopy height model (CHM) to be derived. Full details of the processing are given in [15], but in summary the first and last-return point cloud data were converted to a gridded product using a triangulation algorithm. The last return data were then filtered with an adaptive morphological filter to identify local minima, by varying the filter size based on canopy structural heterogeneity, to create a DTM [29]. The CHM was created by subtracting the DTM from the gridded first return data. The root mean square error (RMSE) for the LiDAR derived products, when assessed against the theodolite data (described in Section II, part B), was 0.51m for the DTM and 1.28m for the CHM [15], [29].

III. DTM GENERATION

Two methods were applied to produce DTMs (Fig. 1). The first, the minimum filtering method, relies upon filtering the InSAR DSM height values to create the DTM from local height minima, which are assumed to originate from the terrain under the vegetation canopy. The ancillary data method is the second method and it exploits various parameters from the PolInSAR data set, plus some derived PolInSAR products, to identify ground pixels (Fig. 1). The ancillary data sets used were coherence and backscatter, plus derived products such as the spatial and spectral standard deviation and fraction of surface scatter derived from a polarimetric decomposition algorithm. The underlying physical principle is that the volume scattering from the canopy layer and the surface scattering from the ground affect the radar signal in specific ways, and consequently radar parameters can be used to infer scattering properties of the target.

The ancillary data sets were incorporated into the DTM generation by applying a threshold to the ancillary data set pixels to create a binary mask with 1 representing "ground" pixels and 0 "non-ground" pixels (Fig. 2). The InSAR height pixels which were identified as "ground" pixels, via the thresholding, were then interpolated to create a terrain surface under the wood. The final stage was the application of a mean filter to smooth the DTM. To identify the most appropriate mean filter size a series of filters with windows of 5, 15, 25, 35, 45, 55 and 65 pixels diameter were tested. To determine the optimum threshold level for each of the ancillary data sets a range of thresholds were also tested, which in conjunction with the 6 InSAR DSM's available and the number of mean filtering options applied led to 1428 DTM being created overall (see Table I). Details of the two methods are described below, including a brief rationale why we expect the ancillary data sources to be able to separate ground pixels from canopy pixels.

A. Minimum filtering

The minimum filtering method uses only the InSAR DSM height values, as the DTM is produced by applying a filter to determine local height minima and then smoothing with a mean filter (Fig. 1; Table I). Six window sizes were tested for the minimum filter, specifically 3x3, 5x5, 7x7, 9x9, 15x15 and 25x25 pixels. After the minimum filtering, to maintain consistency with the ancillary data DTMs, 7 mean filter sizes were applied (square filters of 5, 15, 25, 35, 45, 55 and 65 pixels diameter) producing a total of 252 minimum filtered DTMs (6 input DSMs x 6 minimum filter sizes x 7 mean filters).

B. Data fusion using ancillary data

Backscatter: At L-band the radar signal penetrates the canopy and is scattered primarily by tree branches and trunks, and is unlikely to interact with the ground, if the canopy is dense. Consequently, assuming stable moisture conditions, high biomass canopies generally produce high backscatter and low biomass canopies low backscatter at L-band [30], [31], as a result relatively low backscatter values are assumed to characterize "ground" pixels, which are better suited for inclusion in the DTM generation. The backscatter coefficient was the only logarithmically scaled (and hence non-linear) parameter used. The backscattering coefficient, σ_0, was calculated for the six polarizations (L-HH, L-HV, L-VV, υ_1, υ_2, υ_3) and the thresholding was applied to the dB scaled values (Fig. 2, Table I). Fig. 3a shows the L-HH σ_0 image of Monks Wood, with rides, gaps in the canopy and sparser areas of the canopy exhibiting low backscatter as expected from L-band scattering processes.

Interferometric coherence: The coherence was calculated for the L-HH (Fig. 3b), L-HV, L-VV polarizations and also for the optimized channel polarizations. For the optimized coherence, by definition, υ_1 has the highest coherence and υ_3 the lowest. One consequence of this is that in some cases the υ_3 coherence is too low to reliably determine the InSAR DTM, so it contains more missing pixels than the other channels. We set a coherence threshold of 0.2 below which we did not calculate InSAR height.

Interferometric coherence, for repeat-pass sensors, is a function of the temporal, volume and sensor decorrelation, with the volume decorrelation being important for this application. For predominantly ground pixels we expect only a negligible amount of volume decorrelation, so the interferometric coherence should be relatively high.

Conversely, for canopy pixels we expect high volume decorrelation, due to the large number of scatterers in the canopy, producing relatively low coherence. Temporal decorrelation for volume scatterers within the image is also likely to be increased by the windy conditions at the time of image acquisition, even though the repeat-pass time (13 minutes) was short.

Low coherence may also occur due to low SNR resulting from the very low backscatter observed from smooth surfaces, which would confound our assumption that low coherence implies volume scattering and hence presence of a vegetation canopy. However, this behavior was not observed within the perimeter of the wood. The coherence thresholds applied are detailed in Table I.

Spatial InSAR DSM standard deviation: The spatial standard deviation of the InSAR DSM's for each polarization (L-HH, L-HV, L-VV, υ_1, υ_2, υ_3) was calculated over a 3x3 window. A small window size was chosen to allow detection of small gaps in the canopy. We assumed that the spatial standard deviation of a cluster of bare ground pixels varies less than the canopy height at Monks Wood over an equivalent area, so that a low standard deviation is likely to indicate a cluster of ground pixels, whilst higher values suggest canopy scattering (Table I). This assumption is less robust than the others, as it is not based on the differences between SAR surface and canopy scattering mechanisms and will be discussed later (section V part A). Fig. 3c shows that canopy pixels in the Monks Wood data set have high spatial standard deviation complying with our assumption.

Spectral InSAR DSM standard deviation: The InSAR DSM's for the six polarizations (L-HH, L-HV, L-VV, υ_1, υ_2, υ_3) were used to determine the spectral standard deviation (Fig. 3d). The rationale for using the spectral standard deviation was that ground pixels would have low height standard deviation across the six polarizations, whereas the different polarizations would produce a range of phase scattering heights within the canopy and so a higher standard deviation for canopy hits. The threshold levels are given in Table I.

Surface scatter: The Freeman-Durden model [3] enables decomposition of fully polarimetric SAR data into a combination of three physically based scattering mechanisms, volume scatter, double bounce scatter (e.g. ground-trunk interactions in wooded areas) and rough surface scatter. The decomposition is achieved through a simplified model of the scattering interactions, whereby the canopy scattering is solved for a canopy layer of randomly orientated, thin cylindrical scatterers. Double-bounce scattering is modeled as a dihedral corner reflector, with variable dielectric properties, whilst surface scattering is modeled using a first order Bragg model [3]. The Freeman-Durden decomposition has been successfully used to create ancillary data sets to improve speckle-filtering of PolInSAR data [4].

The Freeman-Durden decomposition was applied to the Monks Wood L-band E-SAR data to estimate the percentage of scattering attributed to each of the three scattering mechanisms. The surface scatter ground pixel selection, along with the spectral standard deviation pixel selection, are independent of polarization, as the same set of ground pixels are used for each polarization (Fig. 3e). For the other methods the set of ground pixels selected will vary slightly depending on polarization, although the number and distribution of points is likely to be highly correlated between different polarizations.

IV. VALIDATION OF THE 1428 DTMS

The accuracy of an interpolated DTM under a vegetation canopy is dependent upon:

1. A sufficient number and even distribution of ground pixels being retained for the interpolation throughout the wood. This is determined by a variety of study site and sensor characteristics, including the scale of terrain variability, the spatial resolution and wavelength of the SAR system and attenuation of the signal in the canopy.
2. Having a suitable method of separating and identifying the ground or predominantly ground pixels from canopy pixels.

The first point is addressed by the validation against the theodolite elevation measurements and LiDAR DTM (described in point i) and iii) below), whilst the second point is addressed using a set of ground pixels derived from the LiDAR CHM.

i) *Accuracy assessment against theodolite data set* - the InSAR DTM's are evaluated against the theodolite terrain elevation data set producing an estimate of the accuracy of the DTM against a high accuracy set of point data.

ii) *Assessment of the pixels selected as ground* – this stage of the assessment procedure is intended to investigate whether the pixels identified as "ground" via the thresholding of the ancillary data sets, really are ground pixels. This was tested using a LiDAR CHM [15] to determine the pixels where the canopy was less than 1.0m tall, which we used as our reference set of ground pixels.

iii) *Spatial distribution of error* – the final stage in the accuracy assessment was to assess the spatial distribution of error for all the pixels, by comparing the InSAR DTM's to the LiDAR DTM [15] and assessing to what extent the InSAR DTM error is influenced by spatial factors, such as incidence angle.

V. RESULTS

A. Accuracy assessment against theodolite data

A summary of the RMSE values, between the theodolite measurements and the best DTM surface (defined as the lowest RMSE against the test data) for each of the methods of DTM generation is given in Table II. The results show that the minimum filter produces the lowest RMSE result (RMSE=4.23m), with the surface scattering method producing the second lowest result (RMSE=4.9m). The optimized coherence υ_2 and υ_3 values produce the best results for most

ancillary data set methods, whereas the L-HH polarized data produce the best overall result, via the minimum filtering method (Table II). Applying different mean filter window sizes to the DTMs typically produced relatively high error for large and small filter windows and reached a minimum at some mid-range filter window size. Generally, the 55x55 pixel mean filter, corresponding to a 165m x 165m window, produces the best result in Table II. This is a relatively coarse filter given the small size of the wood and possibly highlights the low rates of terrain elevation change and the subsequent high levels of spatial autocorrelation within this wood. This is illustrated in Fig. 4a which presents the best results from the minimum filtering and for an ancillary data set (specifically surface scatter) and shows that there is systematic over and under-estimation, presumably as a consequence of the interpolation and filtering stages.

Visual inspection of the distribution of elevation error across the wood showed that at the south-eastern side of the wood the error was particularly high (discussed in section V part C). When the lower accuracy south-eastern theodolite points are excluded from the analysis, the best σ_0 ancillary data DTM is more accurate than the best minimum filter DTM (Table III, Fig. 4b). This suggests that the minimum filter, with the least input data has less error propagation and so is more robust, than the data fusion methods. When the input data are of higher quality, then the data fusion methods may produce better results. It is also noticeable that the range in RMSE values is larger for Table III (1.59m between max. and min. RMSE) than for Table II (0.59m), hence the choice of ancillary data set has less impact on the accuracy of the DTM when assessed against the subset of theodolite points.

The improvement in the InSAR DTM accuracy for the western set of theodolite data is reflected in the reduction of the mean filter size, between Tables II and III. Additionally, with the exception of the spectral standard deviation, all the thresholds change so that the number of pixels, creating the surface to be interpolated, is reduced between the best scenarios in Table II and III. This indicates that a spatially adaptive filter, possibly utilizing the coherence, in conjunction with ground pixels identified from an ancillary data set may improve the accuracy of the interpolated surface further. L-HH and υ_3 consistently produce the highest accuracy DTM's suggesting that they have the strongest scattering response from the ground, within the selected ground pixels.

The weakest rationale underlying the use of any of the ancillary data sets was for the spatial standard deviation, as it was assumed that low values signified a cluster of ground pixels. However, in the quantitative assessment it produces similar results to the coherence data set (Tables II & III).

B. Validation of ground pixel selection

The second stage of validation was to assess whether thresholding the ancillary data sets accurately identified ground pixels. To investigate this we used the LiDAR-derived CHM to identify pixels where the CHM was less than 1m, which we took to be ground pixels. The LiDAR identified ground pixels were then compared with the ground pixels selected by each of the ancillary data set scenarios (threshold and polarization combinations) to identify the highest percentage of accurately identified ground pixels (Table IV). The ancillary data set scenarios identified in Table IV equate to a set of DTM's rather than a specific DTM, so for the backscatter, coherence and spatial standard deviation data sets a set of 7 DTM's is produced, as 7 mean filter sizes were applied (see Fig. 1). Whereas for the spectral standard deviation and the surface scatter data sets, which are polarization independent, the number of DTM for a specified threshold is determined by the number of mean filter sizes (7) and the number of polarizations (6) creating a set of 42 DTM's. Consequently, the RMSE values reported in Table IV are the lowest RMSE values for a set of 7 or 42 DTM.

The maximum percentage of correctly identified ground pixels is 98% for the coherence, although it is based on a small number of pixels and as the RMSE shows produces a very poor set of DTM's. The spectral standard deviation scenario identified coincides with the best spectral standard deviation result identified in Table II for the full theodolite data set. The maximum percentage values for the backscatter and surface scatter data sets were produced by the scenarios that resulted in the highest accuracy in Table III and are based on 3079 and 126 accurate ground pixels respectively. The large difference in the number of accurate ground pixels, between these two cases, has little impact on the ensuing accuracy of the DTM, which may imply the underlying terrain is relatively simple in shape and can be reconstructed relatively accurately from a small number of well-distributed points. The scenarios identified in Table IV coincide occasionally with the best results identified in Tables II and III, however, knowledge of the percentage of accurate ground pixels, or the number of accurate ground pixels does not relate directly to the quality of the final DTM.

C. Comparison of InSAR and LiDAR DTMs

The focus of the final stage of evaluation was to assess the spatial distribution of error in an attempt to understand the limiting factors. The two DTM's with the highest accuracy against the full theodolite data set (Fig. 4a), plus the two DTM's with the highest accuracy against the western subset of points (Fig. 4b), were selected for comparison with the LiDAR DTM. Fig. 5 shows the spatial distribution of error in the four InSAR DTM's, using the LiDAR DTM as a reference data set. The overall pattern of residual error is similar between the 4 DTM's displayed, with error lowest at the northern edge of the wood (near range position) and increasing towards the southern (far range) and eastern edges, although at a finer scale there are distinct differences.

To further investigate the residual error an analysis, with regard to incidence angle, canopy height and each of the ancillary data types (i.e. coherence, backscatter etc.), was

conducted. No relationship between the residual error and the ancillary data sets or canopy height was found. The lack of relationship between residual error and canopy height might appear unexpected, as canopy height and the probability of the radar penetrating the canopy to ground-level are often linked. However, Monks Wood has a dense shrub layer, which has a potentially greater impact on the probability of canopy penetration than the overall height of the canopy, as was found in an earlier LiDAR-based study of Monks Wood [29]. A relationship between incidence angle and residual error was found (Fig. 6), possibly due to increased signal attenuation at higher incidence angles. The mean residual is relatively low between 39° - 45°, before increasing for all but the most coarsely filtered minimum filter DTM. This suggests that the coarse filtering provided some immunity to the effects of incidence angle variations, although beyond 50° all four DTM's show high residual error. Consequently, the error towards the southern edge of the wood (far range) is thought to be due to incidence angle, whereas the error towards the eastern edge may be due to phase unwrapping errors, as the error extends eastwards into the croplands beyond the perimeter of the wood (Fig. 5 a-d).

VI. Discussion

The data fusion method proposed has only been tested at one study site and needs testing at further sites with both airborne and spaceborne data sets. In particular, it requires assessment on larger forested areas, with more varied topography underlying the canopy. It would be worthwhile for the InSAR community to compile an international experimental database containing standardized data sets for a series of test sites, against which to test new algorithms or approaches. The current situation of various approaches being applied to different areas and different InSAR sensors, with varying degrees of validation, makes it difficult to compare methods. Precedents for this have already been set by other remote sensing communities, with the model intercomparison exercise by the optical canopy reflectance modelers [32], [33] and the point cloud filtering experiment conducted by the LiDAR processing community [34]. In addition, work is required to determine a suitable error metric (or set of metrics) for quantifying the accuracy of DTM under forest canopies where the error is very variable spatially.

The use of ancillary data sets to identify ground pixels for use in DTM generation could potentially be extended to use other types of data, both to determine the ground pixels and also to generate the DTM's. If the data are accurately geo-located, then data from other types of remote sensing sensor or even ground data might be suitable for incorporation. For example, optical vegetation indices, such as the normalized difference vegetation index (NDVI) and normalized difference water index (NDWI) could be produced and then thresholded to produce a mask of canopy or non-canopy (or sparse canopy) pixels. One of the key problems would be differences in wavelength and hence canopy penetration, between the radar and optical sensors, as they respond to different biophysical properties [12].

Two of the ancillary data sets tested in this paper can only be derived from a fully polarimetric interferometric data set (e.g. surface scatter, InSAR height standard deviation), whereas the others can be derived from single polarization InSAR data (e.g. coherence, backscatter and spatial standard deviation). The fact that three of the ancillary data products can be generated from a single polarization InSAR data set make the approach suitable for L-band spaceborne InSAR sensors like ALOS-PALSAR [35].

Our motivation for improving the quality of the DTM is to improve the accuracy of canopy height mapping, using X-band InSAR data to map the top of the canopy and an InSAR DTM to map topography [14]. Once an accurate DTM is derived for an area it will not require updating, as frequently as the canopy height, so growth could be monitored by a one-off DTM generation, followed by periodic canopy height measurements with satellite-borne X-band InSAR. Alternatively accurate under-canopy DTM's could be useful in constraining the inversion process in PolInSAR canopy models, enabling alternative parameters to be retrieved in the inversion process.

VII. CONCLUSIONS

In this paper we have proposed a method for using ancillary data sets to determine likely ground pixels within a wood, from which to interpolate a DTM. The results show that the method has promise; in particular, the υ_3 backscattering coefficient to determine ground pixels produces better results than the minimum filtering method, when assessed against a spatial subset of the theodolite data. An analysis of the InSAR DTM's against a LiDAR DTM showed that residual error was correlated to incidence angle, with incidence angles above 50° particularly associated with higher errors. Overall, whilst the method shows some promise it needs applying to other InSAR data sets covering a range of forest and terrain types to provide a full assessment of the method's limitations and robustness. This type of analysis would be greatly facilitated if the InSAR community compiled a standardized series of data sets for different types of forests and sensors against which new algorithms and methods could be tested.

Acknowledgment

We would like to thank Ross Hill and David Gaveau (CEH Monks Wood) who processed and validated the LIDAR data and made the theodolite measurements. Oliver Stebler (RSL, University of Zurich) processed the E-SAR data to create the optimized coherence SLC data set. © E-SAR data by British National Space Center and NERC. LIDAR data are courtesy of the Environment Agency. We thank the reviewers for their helpful comments.

REFERENCES

[1] R. Bamler and P. Hartl, "Synthetic aperture radar interferometry", *Inv. Probl.*, vol. 14, pp. R1-R54, 1998.

[2] S. R. Cloude and E. Pottier, "A review of target decomposition theorems in radar polarimetry", *IEEE Trans. Geosci. Remote Sens.*, vol. 34, no.2, pp. 498-518, Mar. 1996.

[3] A. Freeman and S.L. Durden, "A three-component scattering model for polarimetric SAR data", *IEEE Trans. Geosci. Remote Sens.,* vol. 36, no. 3, pp. 963-973, May 1998.

[4] J.S. Lee, M.R. Grunes, D.L. Schuler, E. Pottier, and L. Ferro-Famil, "Scattering-model-based speckle filtering of polarimetric SAR data", *IEEE Trans. Geosci. Remote Sens.,* vol. 44, pp. 176-186, Jan. 2006.

[5] F. Garestier, P. Dubois-Fernandez, X. Dupuis, P. Paillou, and I. Hajnsek, "PolInSAR analysis of X-band data over vegetated and urban areas", *IEEE Trans. Geosci. Remote Sens.,* vol. 44, no. 2, pp. 356-364, Feb. 2006.

[6] R.Z. Schneider, K. P. Papathanassiou, I. Hajnsek., and A. Moreira., "Polarimetric and interferometric characterization of coherent scatterers in urban areas", *IEEE Trans. Geosci. Remote Sens.,* vol. 44, pp. 971-984, Apr. 2006.

[7] A. Martini, L. Ferro-Famil, E. Pottier, and J.P. Dedieu, "Mapping dry snow in mountain regions from fully polarimetric SAR data", *Proc. PolInSAR 2005,* ESA, ESRIN, Frascati, Italy (on CD-ROM), Jan. 2005.

[8] S.R. Cloude and K.P. Papathanassiou, "Polarimetric SAR interferometry", *IEEE Trans. Geosci. Remote Sens.,* vol. 36, no. 5, pp.1551-1565, Sep. 1998.

[9] R.N. Treuhaft and P.R. Siqueira, "Vertical structure of vegetated land surfaces from interferometric and polarimetric radar", *Radio Sci.,* vol. 35, no. 1, pp. 141-177, 2000.

[10] K.P. Papathanassiou and S.R. Cloude, "Single-baseline polarimetric SAR interferometry", *IEEE Trans. Geosci. Remote Sens.,* vol. 39, no. 11, pp. 2352-2363, Nov. 2001.

[11] R.N. Treuhaft, S.N. Madsen, M. Moghaddam, and J.J. van Zyl, "Vertical structure of vegetated land surfaces from interferometric and polarimetric radar", *Radio Sci.,* vol. 31, no. 6, pp. 1449-1485, 1996.

[12] R.N. Treuhaft, B.E. Law, and G.P. Asner, "Forest attributes from radar interferometric structure and its fusion with optical remote sensing data", *Bioscience,* vol. 54, no. 6, pp. 561-571, June 2004.

[13] H.E. Andersen, R.J. McGaughey, W.W. Carson, S.E. Reutebuch, B. Mercer, and J. Allan, "A comparison of forest canopy models derived from LIDAR and INSAR data in a Pacific Northwest conifer forest", *Int. Archives of Photogram. and Rem. Sens.*, vol. 34(Part 3/W13), pp.211-217, 2003.

[14] H. Balzter, C.S. Rowland, and P. Saich, "Forest canopy height and carbon estimation at Monks Wood national Nature Reserve, UK, using dual-wavelength SAR interferometry", *Remote Sens. Environ*., submitted for publication.

[15] D. L. A. Gaveau and R. A. Hill, **"**Quantifying canopy height underestimation by laser pulse penetration in small-footprint airborne laser scanning data"**,** *Can. J. of Remote Sensing,* vol. 29, no. 5, pp. 650-657, Oct. 2003.

[16] J. Kellndorfer, W. Walker, L. Pierce, C. Dobson, J.A. Fites, C. Hunsaker, J. Vona, and M. Clutter, "Vegetation height estimation from Shuttle Radar Topography Mission and National Elevation Datasets", *Remote Sensing of Environment,* vol. 93, no. 3, pp. 339-358, Nov. 2004.

[17] Izzawati, E.D. Wallington, and I.H. Woodhouse, "Forest height retrieval from commercial X-band SAR products", *IEEE Trans. Geosci. Remote Sens.,* vol. 44, no. 4, pp. 863-870, Apr. 2006.

[18] D.B. Gesch, J.-P. Muller, and T.G. Farr, "The Shuttle Radar Topography Mission – Data validation and applications", *Photogram. Eng. Remote Sens.,* vol. 72, no. 3, pp. 233-235, Mar. 2006.

[19] M.D. Coleman and J.B. Mercer, "NEXTMap Britain: Completing Phase 1 of Intermap's Global Mapping Strategy", *GeoInformatics*, vol. 5, no. 12, pp. 16-19, Dec. 2002.

[20] Y. Zhang, C.V. Tao, and J.B. Mercer, "An initial study on automatic reconstruction of ground DTMs from airborne IfSAR DSMs", *Photogram. Eng. Remote Sens.,* vol. 70, no. 4, pp. 427-438, Apr. 2004.

[21] K. Kraus and N. Pfeifer, "Determination of terrain models in wooded areas with airborne laser scanning data", *ISPRS J. Photogram. Remote Sens.*, vol. 53, no. 4, pp. 193-203, Aug. 1998.

[22] M.E. Hodgson, J.R. Jensen, L. Schmidt, S. Schill, and B. Davis, "An evaluation of LIDAR- and IFSAR-derived digital elevation models in leaf-on conditions with USGS Level 1 and Level 2 DEMs", *Remote Sens. Environ.,* vol. 84, no. 2, pp. 295-308, Feb. 2003.

[23] S.E. Reutebuch, R.J. McGaughey, H.E. Andersen, and W.W Carson, "Accuracy of a high-resolution lidar terrain model under a conifer forest canopy", *Canadian J. Remote Sens.,* vol. 29, no. 5, pp. 527-535, Oct. 2003.

[24] M.E. Hodgson, J.R Jensen, G. Raber, J. Tullis, B. Davis, K. Schuckman, and G. Thompson, "An Evaluation of LIDAR-Derived Elevation and Terrain Slope in Leaf-off Conditions", *Photogram. Eng. and Remote Sens.*,, vol. 71, no.7, pp. 817-823, Jul. 2005.

[25] M. Gelautz, P. Paillou, C.W. Chen, and H.A. Zebker, "Radar stereo- and interferometry-derived digital elevation models: comparison and combination using Radarsat and ERS-2 imagery", *Int. J. Remote Sens.*, vol. 24, no. 24, pp. 5243 – 5264, Dec. 2003.

[26] F. Rottensteiner, J. Trinder, S. Clode, and K. Kubik, "Using the Dempster-Schafer method for the fusion of LIDAR data and multi-spectral images for building detection", *Information Fusion,* vol. 6, no. 1, pp. 283-300, Mar. 2005.

[27] R.C. Steele, and R.C. Welch, *Monks Wood: A nature reserve record*. Cambridge, UK: The Nature Conservancy, 1973, 337 pp.

[28] O. Stebler, E. Meier, and D. Nüesch, "Multi-baseline polarimetric SAR interferometry-first experimental spaceborne and airborne results", *ISPRS J. Photogram. Remote Sens.*, vol. 56, no. 3, pp.149-166, Apr. 2002.

[29] R.A. Hill, S.A. Hinsley, and D.L.A. Gaveau, "Mapping forest pattern and structure at a landscape scale using airborne laser scanning technology", *IALE 2002, Avian Landscape Ecology,* Sept. 2002.

[30] M.C. Dobson, F.T. Ulaby, T. Le Toan, A. Beaudoin, E.S. Kasischke, and N. Christensen, "Dependence of radar backscatter on coniferous forest biomass, *IEEE Trans. Geosci. Remote Sens.,* vol. 30, no, 2, pp. 412-415, Mar. 1992.

[31] M.L. Imhoff, "A theoretical analysis of the effect of forest structure on Synthetic Aperture Radar backscatter and the remote sensing of biomass", *IEEE Trans. Geosci. Remote Sens.,* vol. 33, no. 2, pp. 341-352, Mar. 1995.

[32] B. Pinty, N. Gobron, J.-L. Widlowski, S.A.W. Gerstl, M.M. Verstraete, M. Antunes, C. Bacour, F. Gascon, J.-P. Gastellu-Etchegorry, N., Goel, S. Jacquemoud, P. North, W. Qin, and R. Thompson, "Radiation transfer model intercomparison (RAMI) exercise", *J. Geophy. Res.*, vol. 106, pp. 11937-11956, 2001.

[33] B. Pinty, J.-L. Widlowski, M. Taberner, N. Gobron, M.M. Verstraete, M. Disney, F Gascon, J.-P Gastellu, L., Jiang, A. Kuusk, P. Lewis, X. Li, W. Ni-Meister, T. Nilson, P. North, W. Qi, L. Su, S. Tang, R. Thompson, W. Verhoef, H. Wang, J. Wang, G. Yan, H. Zang, "Radiation transfer model intercomparison (RAMI) exercise: Results from the second phase", *J. Geophy. Res.*, vol. 109, D06210, 2004.

[34] G. Sithole and G. Vosselman, "Experimental comparison of filter algorithms for bare-Earth extraction from airborne laser scanning point clouds", *ISPRS J. Photo. Remote Sens.*, vol. 59, pp. 85-101, Aug. 2004.

[35] M. Shimada, A. Rosenqvist, M. Watanbe, and T. Tadano, "The polarimetric and interferometric potential of ALOS-PALSAR", *Proc. PolInSAR 2005,* ESA, ESRIN, Frascati, Italy (on CD-ROM), Jan. 2005.

Clare S. Rowland received a B.Sc. in Environmental Science and a M.Sc. in Remote Sensing from the University of London, UK in 1995 and 1997 respectively, followed by a Ph.D. in remote sensing from the University of Salford, UK in 2001, for a thesis on the estimation of forest LAI from optical remote sensing data.

She worked at the Environmental Change Institute of the University of Oxford from 2000-2002 on carbon and biomass estimation from remote sensing. She then joined the Section for Earth Observation at the Centre of Ecology and Hydrology Monks Wood, where her research has covered burnt area mapping in Siberia, investigating airborne PolInSAR for retrieving biophysical variables from coniferous and deciduous woodland, and the use of remote sensing products for assessment of forest condition.

Heiko Balzter received a Diplom (MSc equivalent) in 1994 with a dissertation topic on methods for vegetation sampling and a PhD in 1998 from Justus-Liebig-University in Giessen, Germany, for a thesis on vegetation modeling using Markov Chains and Cellular Automata.

He is Professor in Physical Geography at the University of Leicester, UK, and has research interests in biosphere / climate interactions and their responses to environmental change, with a focus on remote sensing and

modeling approaches. From 1998 to 2006 he worked for the Centre for Ecology and Hydrology, Monks Wood, UK, for the final three years as Head of Section for Earth Observation. He has been involved in major international remote sensing research projects like SIBERIA, SIBERIA-2 and GEOLAND.

Professor Balzter is a member of the Senior Management Committee of the NERC Climate and Land Surface Systems Interaction Centre, an Earth Observation Centre of Excellence, an elected member of the International Geosphere Biosphere Programme (IGBP) UK National Committee, expert reviewer for the 4th Intergovernmental Panel on Climate Change (IPCC) Assessment Report (WG2 and WG3), member of the AATSR Science Advisory Group, fellow of the Royal Statistical Society and Royal Geographical Society, member of the Northern Eurasian Earth Science Partnership Initiative (NEESPI), and the Siberia Earth System Science Cluster (SIBESSC). He is peer reviewer for 12 journals including IEEE Transactions on Geoscience and Remote Sensing.

TABLE 1

RANGE, THRESHOLDS AND INCREMENTS FOR SELECTION OF POTENTIAL GROUND PIXELS FROM ANCILLARY DATA SETS. THE NUMBER OF DTM'S GENERATED WAS CALCULATED AS: NUMBER OF INCREMENTS NUMBER OF CHANNELS (I.E. 6 POLARISATIONS IN ALL CASES) X NUMBER OF MEAN FILTER SIZES TESTED (7 IN ALL CASES).

Method	Minimum threshold	Maximum threshold	Increment	Number of increments	Ground expected to produce:	Number of DTM's generated
Minimum filtering	n/a	n/a	n/a	n/a	n/a	252
Backscatter coefficient	-22.5dB	-12.5dB	-2.5dB	5	Low values	210
Coherence	> 0.3	> 0.9	0.1	7	High values	294
Spectral standard deviation	0.5m	2.5m	0.5m	5	Low values	210
Spatial standard deviation	0.5m	2.5m	0.5m	5	Low values *(assuming cluster of ground pixels)*	210
Surface scatter	>0.2	>0.7	0.1	6	High values	252

TABLE 2

RMSE BETWEEN THE *FULL SET* OF THEODOLITE ELEVATION MEASUREMENTS AND THE MOST ACCURATE DTMS FROM EACH OF THE METHODS, PLUS DETAILS OF THE POLARISATION, FILTER SIZE AND THRESHOLD PRODUCING THE BEST RESULT.

Method	RMSE (m)	Polarization	Mean filter	Threshold
Minimum filter	4.23	L-HH	55	Minimum filter size 9x9
Backscatter	5.39	υ_3	25	<-20.0dB
Coherence	5.82	υ_2	55	>0.3
Spatial standard deviation	5.75	υ_2	55	<2.5
Spectral standard deviation	5.48	υ_3	55	<0.5m
Surface scatter	4.9	υ_3	55	>0.6

TABLE 3
RMSE BETWEEN THE *WESTERN SET* OF THEODOLITE ELEVATION MEASUREMENTS AND THE MOST ACCURATE DTMS FROM EACH OF THE METHODS, PLUS DETAILS OF THE POLARISATION, FILTER SIZE AND THRESHOLD PRODUCING THE BEST RESULT.

Method	RMSE (m)	Polarization	Mean filter	Threshold
Minimum filter	3.37	L-HH	35	Minimum filter size 3x3
Backscatter	2.97	υ_3	35	<-22.5dB
Coherence	3.56	L-HH	35	>0.30
Spatial standard deviation	3.50	L-HH	25	<5
Spectral standard deviation	3.53	υ_3	25	<1.0m
Surface scatter	3.41	L-HH	55	>0.70

TABLE 4
SCENARIOS PRODUCING THE HIGHEST PERCENTAGE OF ACCURATELY IDENTIFIED GROUND PIXELS (DEFINED AS THOSE PIXELS WHERE THE LIDAR-DERIVED CHM IS < 1M) FOR EACH OF THE ANCILLARY DATA SETS.

Method	Highest percentage of accurate ground pixels	Number of accurate ground pixels	Scenario for highest percentage of accurate ground pixels		Lowest RMSE for range of DTM fitting scenario	
			Threshold	Polarization	All theodolite points	Western theodolite points only
Backscatter	51	3079	<- 22.5dB	υ_3	6.00m	2.97m
Coherence	98	81	> 0.90	υ_3	18.10m	22.89m
Spatial standard deviation	24	6681	< 0.5m	υ_3	6.29m	4.38m
Spectral standard deviation	20	5178	< 0.5m	n/a	5.48m	3.60m
Surface scatter	30	126	> 0.70	n/a	6.45m	3.41m

FIGURES

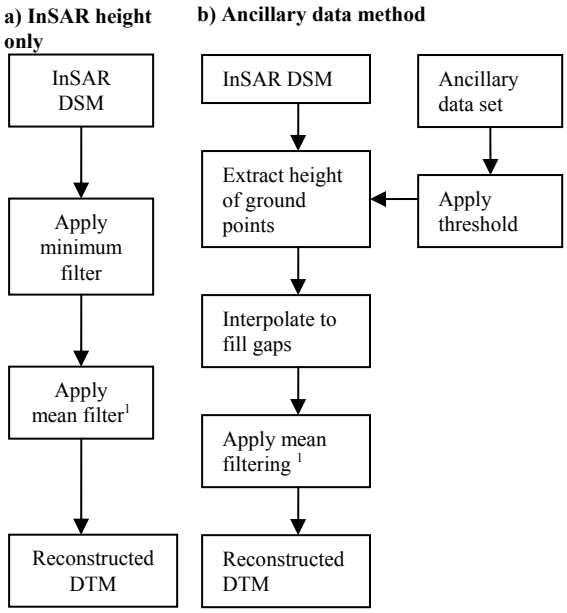

Fig. 1. The two basic methods applied to create the ground DTM using a) height information only, and b) data synergy between InSAR DSM and a variety of additional data sets. [1] The mean filtering was conducted with a series of square filters of: 5, 15, 25, 35, 45, 55 and 65 pixels diameter.

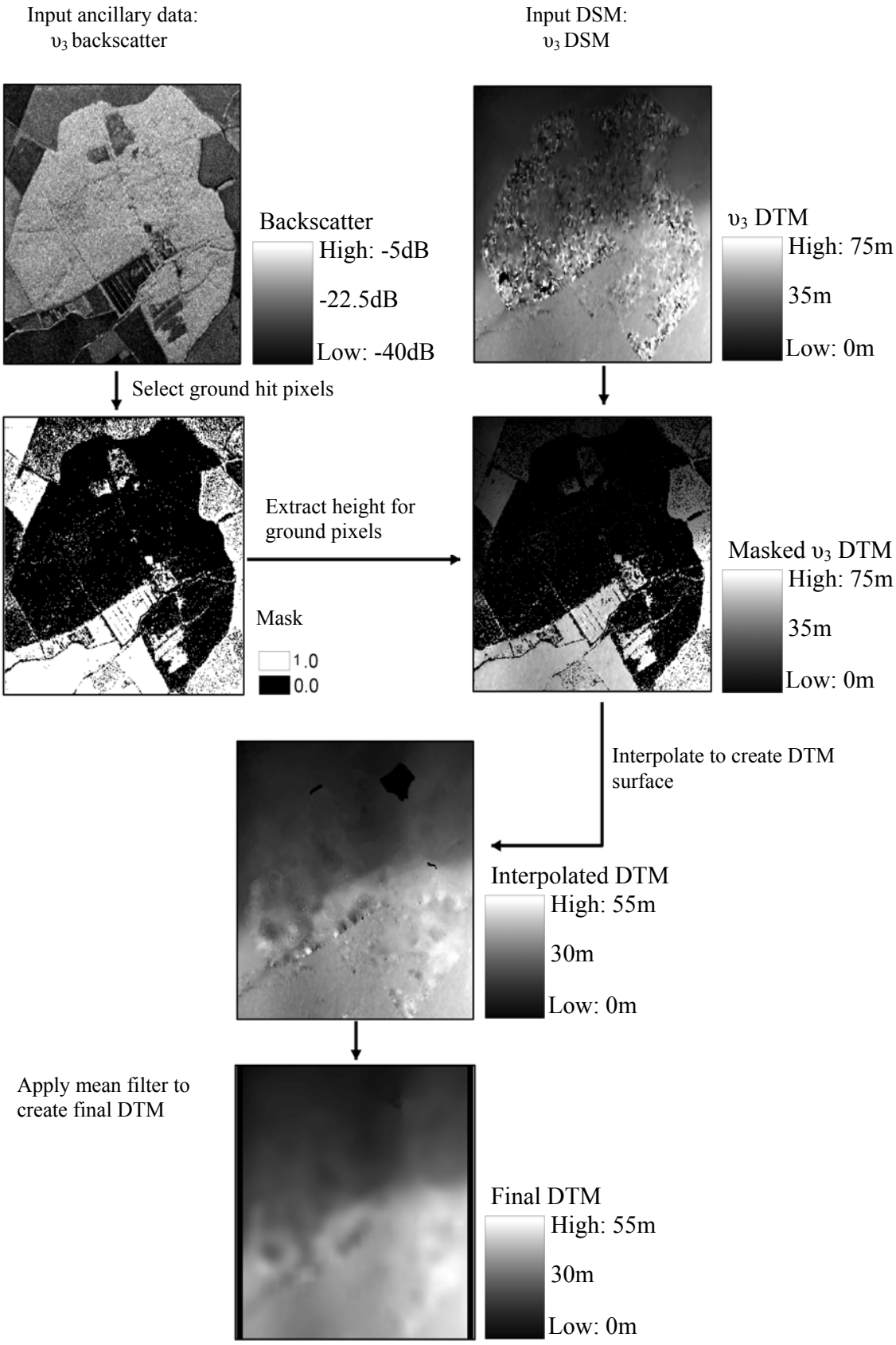

Fig. 2. Illustrated schematic of the data processing chain for the data fusion method, using SAR backscatter as the ancillary data source and the υ_3 DTM as the input elevation values.

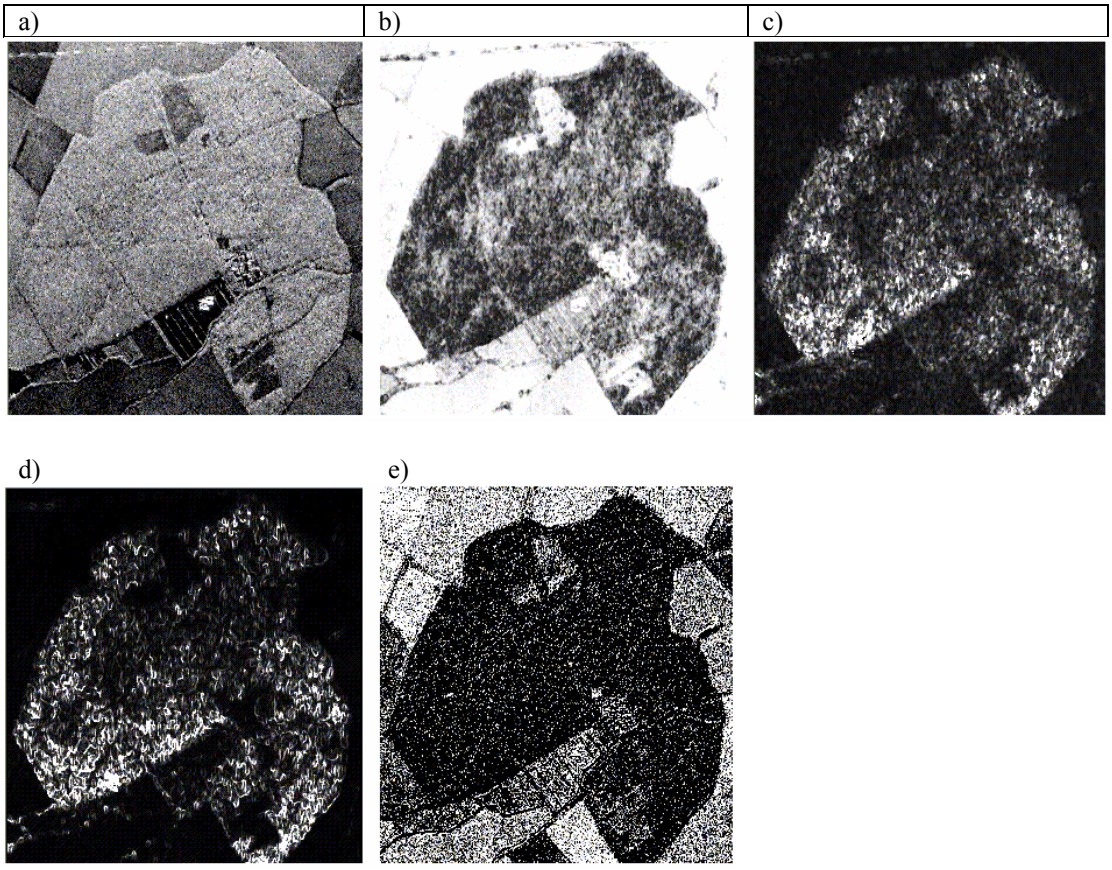

Fig. 3. The ancillary data products for Monks Wood (image centred on: 52°24'N, 0°14'E; image width = 1.8km; image height=2km). (North (top of image) is near-range; south (bottom) is far-range).

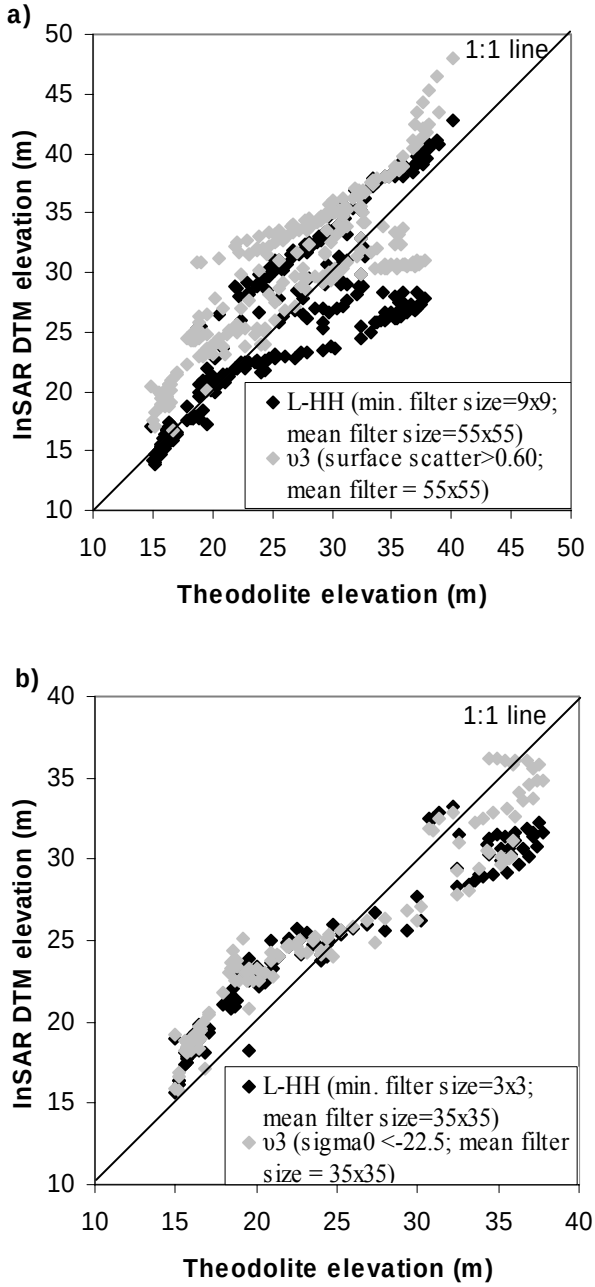

Fig. 4. Validation of InSAR DTM elevation for the two best DTM in the comparison with a) all the theodolite points (Table 2) and b) western set of theodolite points (Table 3). Legend in graph gives minimum filter and mean filter size for minimum filter method; or ancillary data seta and threshold, plus mean filter size for data fusion method.

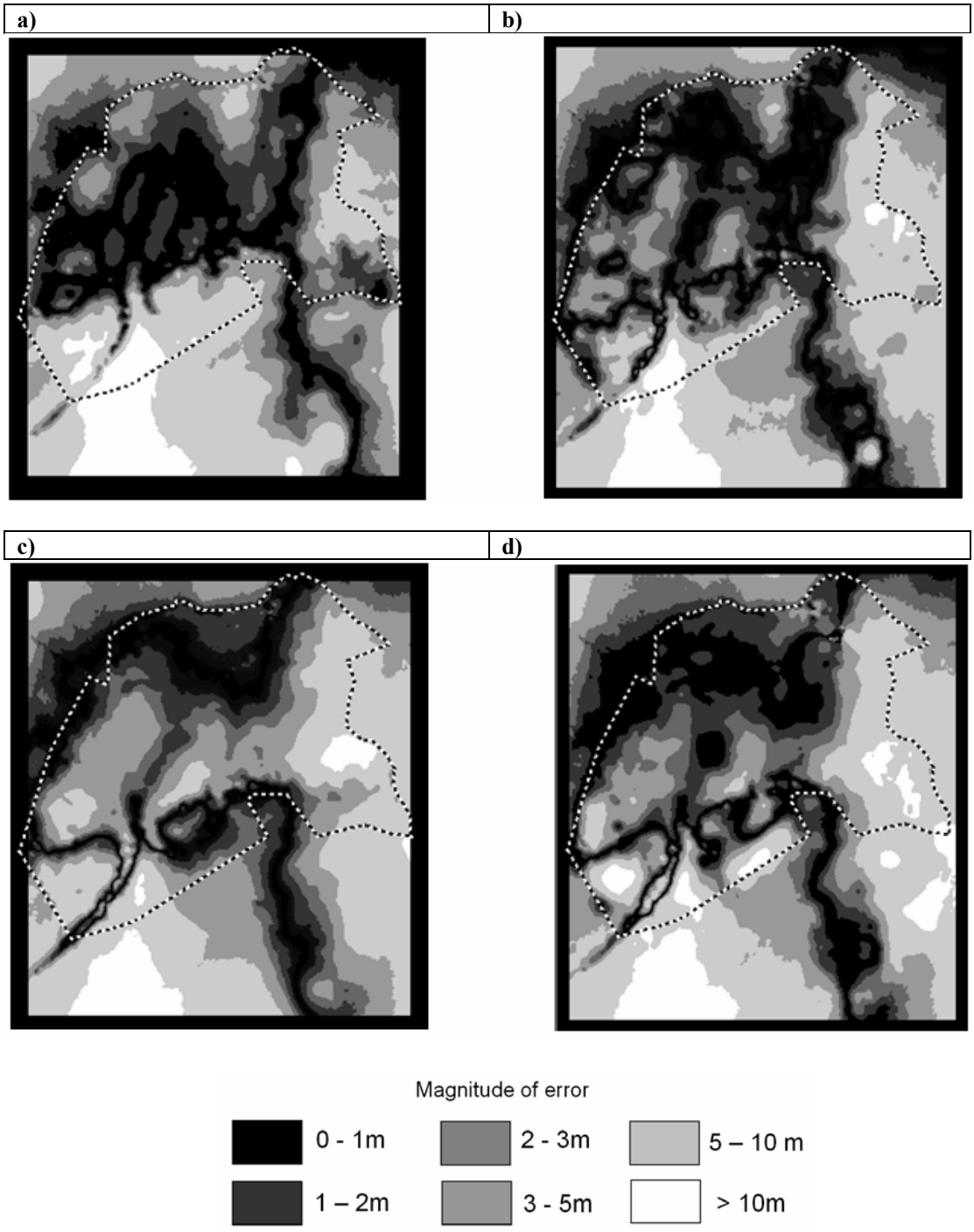

Fig. 5. Spatial distribution of error from a comparison of the LiDAR DTM and four selected InSAR DTMs for Monks Wood. The perimeter of the wood is shown by the dotted line, whilst the black border around the image signifies no data and is an artefact of the filtering. Details on the processing method are in brackets for the images, with minimum filter and mean filter size for minimum filter method; or ancillary data seta and threshold, plus mean filter size for data fusion method.

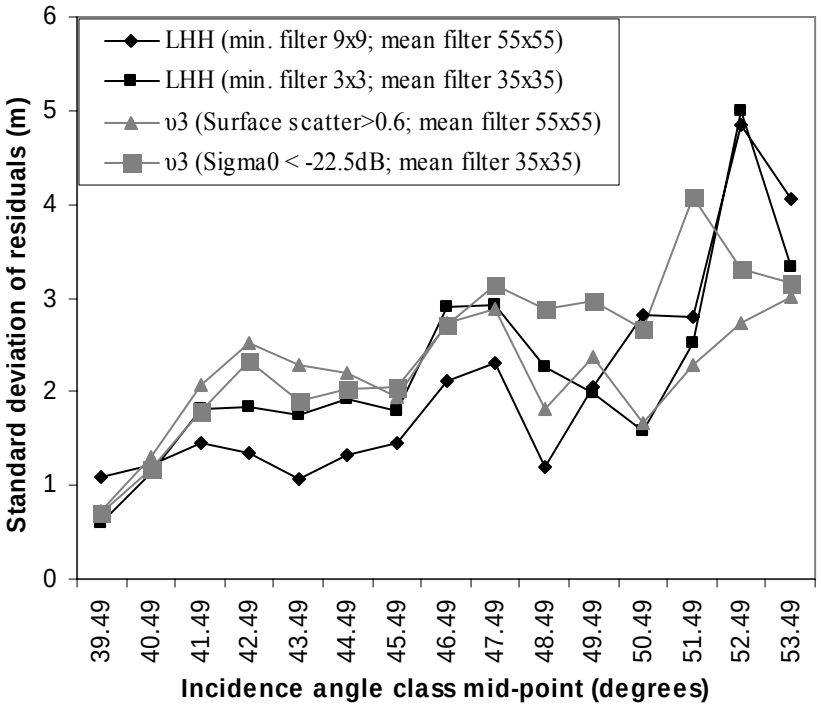

Fig. 6. Relationship between residual error and incidence angle for selected Monks Wood DTM derived from InSAR data.